16

Advanced Numerical Methods for non-Premixed Flames

Annarita Viggiano
Department of Environmental Engineering and Physics
University of Basilicata
Italy

1. Introduction

Engine designers are under increasing pressure to reduce emissions and pollutants. Multidimensional models, as well as advanced experimental techniques, provide fundamental knowledge to meet regulations in terms of efficiency and emissions.
Recently, considerable efforts have been addressed to develop advanced numerical techniques and comprehensive theoretical models, in order to study the dynamic of flames under the operating conditions typical of internal combustion engines, aircraft engines, gas turbine combustors, etc. (Bilger *et al*., 2005; Hilbert *et al*., 2004). Dealing with high Reynolds number reactive flows, invaluable knowledge can be achieved by using accurate numerical methodologies, such as Large-Eddy Simulation (LES) (Pitsch, 2006) and Direct Numerical Simulation (DNS) (Moin & Mahesh, 1998). The frontier research in this field concerns the coupling of such techniques with proper combustion models, in order to study engineering combustion devices fueled by conventional hydrocarbons, hydrogen and renewable bio-based fuels.
In this work, a DNS methodology, coupled with detailed kinetic mechanisms for fuel oxidation, is described. This technique is implemented in an in-house developed CFD software package for the analysis of multicomponent free shear flows (Magi, 2004). Such a tool solves the Navier-Stokes equations for reacting flows by using a detailed description of thermal and transport properties and an accurate modelling of chemical source terms. A high order compact finite difference scheme is adopted for the solution of the partial differential equations (Lele, 1989; 1992). Although the computational code is able to perform both LES and DNS analysis, the latter is used in this work. MPI libraries are employed to fully parallelize the code, thus allowing to execute the computations on high performance parallel machines.
In this contribution, the software package is used to simulate the reacting mixing layer between two streams of air and fuel with different velocity, even though the same methodology has been used to simulate other interesting phenomena for the study of combustion systems, such as the autoignition of fuel in starting transient jets (Viggiano & Magi, 2004; Viggiano, 2009). The role of some physical parameters, such as the mixture fraction, the scalar dissipation rate and the initial conditions, in terms of temperature and velocity, has been explored. The localization of the ignition spots and the ignition delay time have been investigated and the results have been compared with those of several experimental and numerical works in the literature (Mastorakos *et al*., 1997; Mastorakos, 2009; Sreedhara & Lakshmisha, 2000). Besides,

the importance of using a detailed reaction mechanism for a better understanding of the phenomena has been addressed (Viggiano, 2009). The most important findings are summarized in this contribution. Some works in the literature are referred to for further reading.
This chapter is organized as follows. First of all, the mathematical model and the numerical method are given. Then, the computational setup is described. Finally, the results are discussed and the conclusions are summarized.

2. The mathematical model

2.1 The governing equations

The flow field is computed by solving the mass, momentum and energy conservation equations for a compressible, multicomponent mixture of thermally perfect gases. Although the software package solves these equations both in three-dimensional and in two-dimensional configuration, the latter is used in this work. Hence, the governing equations read

$$\frac{\partial \mathbf{W}}{\partial t} + \frac{\partial (\mathbf{F}_\mathrm{E} - \mathbf{F}_\mathrm{V})}{\partial x} + \frac{\partial (\mathbf{G}_\mathrm{E} - \mathbf{G}_\mathrm{V})}{\partial y} + \mathbf{S} = 0, \tag{1}$$

where $\mathbf{W}$ is the unknown vector, the symbols $\mathbf{F}$ and $\mathbf{G}$ stand for the fluxes along x and y directions, respectively, the subscripts E and V relate to the convective and diffusive terms, respectively, while $\mathbf{S}$ stands for the source term.
The unknown vector is defined as

$$\mathbf{W} = \left[\rho_i, \rho u, \rho v, \rho E\right]^T, \tag{2}$$

where ρ_i is the density of the i-*th* chemical species, ρ is the mixture density computed as

$$\rho = \sum_{i=1}^{N_s} \rho_i, \tag{3}$$

where N_s is the total number of the chemical species, u and v are the Cartesian components of the velocity vector $\mathbf{u}$ and E is the total specific energy, given by

$$E = \sum_{i=1}^{N_s} Y_i e_i + \frac{u^2 + v^2}{2}. \tag{4}$$

In Eq. 4 Y_i and e_i are the mass fraction and the internal specific energy of the i-*th* chemical species, respectively.
The convective fluxes are given by

$$\mathbf{F}_\mathrm{E} = \left[\rho_i u, \rho u^2 + p, \rho uv, \rho uH\right]^T \tag{5}$$

$$\mathbf{G}_\mathrm{E} = \left[\rho_i v, \rho uv, \rho v^2 + p, \rho vH\right]^T, \tag{6}$$

where p is the pressure and H is the total specific enthalpy, equal to

$$H = E + \frac{p}{\rho}. \tag{7}$$

The diffusive terms are

$$(\mathbf{F}_\mathrm{V}, \mathbf{G}_\mathrm{V}) = \left[-\rho_i \mathbf{u_i}, \underline{\underline{\tau}}, \mathbf{u} \cdot \underline{\underline{\tau}} - \mathbf{q}\right]^T, \tag{8}$$

with

$$\rho_i \mathbf{u_i} = -\rho D_i \nabla Y_i \tag{9}$$

$$\underline{\underline{\tau}} = \mu \left[\nabla \mathbf{u} + (\nabla \mathbf{u})^T \right] - \frac{2}{3} \mu \nabla \cdot \mathbf{u} \mathbf{I} \tag{10}$$

$$\mathbf{q} = -\lambda_t \nabla T + \sum_{i=1}^{N_s} h_i \rho_i \mathbf{u_i}, \tag{11}$$

where D_i and h_i are the diffusion coefficient and the static enthalpy of the i-*th* chemical species, respectively, μ is the molecular viscosity, λ_t is the thermal conductivity and T is the temperature. Equation 9, that models the diffusion of the generic chemical compound into the mixture, is a generalization of Fick's law for binary mixtures.
The source term reads

$$\mathbf{S} = \left[-\dot{W}_i, 0, 0, 0 \right]^T, \tag{12}$$

where $\dot{W}_i$ is the partial density change rate of the i-*th* chemical species due to chemical reactions. By considering a q-*th* generic reaction in the form

$$\sum_{i=1}^{N_s} \nu_{iq}^{'} C_i \leftrightarrow \sum_{i=1}^{N_s} \nu_{iq}^{''} C_i \quad q = 1, ..., N_R, \tag{13}$$

where, for each chemical species i, $\nu^{'}$ and $\nu^{''}$ are the forward and reverse stoichiometric coefficients, respectively, the symbol C stands for the generic chemical species and N_R is the total number of reactions, $\dot{W}_i$ is given by (Glassman, 1996; Kuo, 2005)

$$\dot{W}_i = M_i \sum_{q=1}^{N_R} \left(\nu_{iq}^{''} - \nu_{iq}^{'} \right) \left(k_{fq} \prod_{l=1}^{N_s} [X_l]^{\delta_{lq}^{'}} - k_{rq} \prod_{l=1}^{N_s} [X_l]^{\delta_{lq}^{''}} \right), \tag{14}$$

where M_i is the molecular weight of the i-*th* chemical species, k_{fq} and k_{rq} are the forward and reverse rate constants of the q-*th* reaction, $[X_l]$ is the molar concentration of the l-*th* chemical species, while $\delta^{'}$ and $\delta^{''}$ are the reaction orders in the forward and reverse direction, respectively. By using the Arrhenius expression, the forward and reverse rate constants for the q-*th* reaction are written as

$$k_q = A_q T^{\beta_q} \exp\left(\frac{-E_{aq}}{RT} \right), \tag{15}$$

where A_q is the pre-exponential factor, β_q is the temperature exponent, E_{aq} is the activation energy and R is the universal gas constant.
The pressure is computed by means of the equation of state

$$p = T \sum_{i=1}^{N_s} \rho_i R_i, \tag{16}$$

where R_i is the gas constant for the i-*th* chemical species.

2.2 The transport and thermodynamic properties

The transport properties of the multicomponent mixture are computed by using Wilke's law (Coffee & Heimerl, 1981; Hirschfelder *et al.*, 1964). The viscosity and the thermal conductivity of the mixture are given by

$$\mu = \sum_{i=1}^{Ns} \frac{\mu_i}{1 + \sum_{j \neq i} \phi_{ij} \frac{X_j}{X_i}} \tag{17}$$

$$\lambda_t = \sum_{i=1}^{Ns} \frac{\lambda_{ti}}{1 + 1.065 \sum_{j \neq i} \phi_{ij} \frac{X_j}{X_i}} \tag{18}$$

where μ_i, λ_{ti} and X_i are the viscosity, the thermal conductivity and the mole fraction of the i-*th* chemical species, respectively, while ϕ_{ij} is given by

$$\phi_{ij} = \frac{1}{8^{\frac{1}{2}}} \left(1 + \frac{M_i}{M_j}\right)^{-\frac{1}{2}} \left[1 + \left(\frac{\mu_i M_j}{\mu_j M_i}\right)^{\frac{1}{2}} \left(\frac{M_i}{M_j}\right)^{\frac{1}{4}}\right]^2. \tag{19}$$

The diffusion coefficient of the i-*th* chemical species in the mixture is given by

$$D_i = \frac{1 - X_i}{\sum_{j \neq i} \frac{X_j}{D_{ij}}}, \tag{20}$$

where D_{ij} is the binary diffusion coefficient.

The properties of the pure species, i.e. μ_i, λ_{ti} and D_{ij}, are computed according to the classic kinetic theory (Hirschfelder *et al.*, 1964).

In the computation of the thermodynamic properties, the gas is assumed to be thermally perfect, hence enthalpy and internal energy only depend on temperature. Following Gordon & McBride (1971), the specific heat at constant pressure for the i-*th* chemical species is given by a polynomial temperature curve fit

$$c_{pi} = \left(a_i + b_i T + c_i T^2 + d_i T^3 + e_i T^4\right) R_i, \tag{21}$$

where R_i is the gas constant for the i-*th* chemical species. As

$$dh_i = c_{pi} dT, \tag{22}$$

the enthalpy is given by

$$h_i = \left(a_i T + \frac{b_i}{2} T^2 + \frac{c_i}{3} T^3 + \frac{d_i}{4} T^4 + \frac{e_i}{5} T^5 + f_i\right) R_i. \tag{23}$$

The polynomial coefficients are given by Gordon & McBride (1971). Two sets of seven polynomial coefficients are used; the first one reproduces the thermodynamic properties for the high range of temperatures ($1000 - 5000$ K), whereas the second set is relative to the low range of temperatures ($300 - 1000$ K). Finally, the thermodynamic properties of the mixture are computed as

$$c_p = \sum_{i=1}^{N_S} c_{pi} Y_i \tag{24}$$

$$h = \sum_{i=1}^{N_S} h_i Y_i. \tag{25}$$

3. The numerical method

3.1 The spatial discretization

The governing equations are discretized by using a compact finite difference scheme, which is a generalization of the classical Padé scheme (Abraham & Magi, 1997; Lele, 1992; Poinsot & Lele, 1992). In each computational grid point, (i, j), the first (second) derivative of a generic variable f is written as a function of the values of f and its first (second) derivatives in the neighbouring grid points. This technique is an attempt to reproduce, by means of a finite difference scheme, the features of spectral techniques. Indeed, such a scheme has a formal accuracy comparable, in a wide range of wavenumbers, to that of spectral approaches.
For a uniform mesh with mesh size h, the first and second derivative expressions along direction i are

$$\begin{aligned}\beta f'_{i-2}+\alpha f'_{i-1}+f'_i+\alpha f'_{i+1}+\beta f'_{i+2}=\\ a\frac{f_{i+1}-f_{i-1}}{2h}+b\frac{f_{i+2}-f_{i-2}}{4h}+c\frac{f_{i+3}-f_{i-3}}{6h}\end{aligned} \tag{26}$$

$$\begin{aligned}\beta f''_{i-2}+\alpha f''_{i-1}+f''_i+\alpha f''_{i+1}+\beta f''_{i+2}=\\ a\frac{f_{i+1}-2f_i+f_{i-1}}{h^2}+b\frac{f_{i+2}-2f_i+f_{i-2}}{4h^2}+c\frac{f_{i+3}-2f_i+f_{i-3}}{9h^2},\end{aligned} \tag{27}$$

where the subscript j is removed for the sake of clarity. By using the Taylor series expansion and imposing the scheme to be sixth order accurate, the following relations between the coefficients are obtained

first derivative

$$\begin{aligned}a+b+c&=1+2\alpha+2\beta\\ a+2^2b+3^2c&=2\frac{3!}{2!}\left(\alpha+2^2\beta\right)\\ a+2^4b+3^4c&=2\frac{5!}{4!}\left(\alpha+2^4\beta\right)\end{aligned} \tag{28}$$

second derivative

$$\begin{aligned}a+b+c&=1+2\alpha+2\beta\\ a+2^2b+3^2c&=\frac{4!}{2!}\left(\alpha+2^2\beta\right)\\ a+2^4b+3^4c&=\frac{6!}{4!}\left(\alpha+2^4\beta\right).\end{aligned} \tag{29}$$

With the above relations, Eqs. 26 and 27 become families of two parameters schemes. For three-diagonal schemes ($\beta = 0$) and right hand size stencil equal to 5 ($c = 0$), the following values of the coefficients are obtained

first derivative

$$\alpha=\frac{1}{3},\beta=0,a=\frac{14}{9},b=\frac{1}{9},c=0 \tag{30}$$

second derivative

$$\alpha=\frac{2}{11},\beta=0,a=\frac{12}{11},b=\frac{3}{11},c=0. \tag{31}$$

In the computational nodes near the boundaries Eqs. 26 and 27 still apply with the following values of the coefficients (classical Padé scheme with fourth order accuracy)

first derivative

$$\alpha = \frac{1}{4}, \beta = 0, a = \frac{3}{2}, b = 0, c = 0 \tag{32}$$

second derivative

$$\alpha = \frac{1}{10}, \beta = 0, a = \frac{6}{5}, b = 0, c = 0. \tag{33}$$

In the boundary nodes $i = 1$ and $i = N + 1$, one side relations are used

$$f_1^{'} + \alpha f_2^{'} = \frac{1}{h}\left(a f_1 + b f_2 + c f_3 + d f_4\right), \tag{34}$$

$$f_{N+1}^{'} + \alpha f_N^{'} = \frac{1}{h}\left(-a f_1 - b f_2 - c f_3 - d f_4\right), \tag{35}$$

$$f_1^{''} + \alpha f_2^{''} = \frac{1}{h^2}\left(a f_1 + b f_2 + c f_3 + d f_4 + e f_5\right), \tag{36}$$

$$f_{N+1}^{''} + \alpha f_N^{''} = \frac{1}{h^2}\left(a f_1 + b f_2 + c f_3 + d f_4 + e f_5\right). \tag{37}$$

In order to obtain a third order accuracy, the following values of the coefficients are employed

first derivative

$$\alpha = 2, a = -\frac{5}{2}, b = 2, c = \frac{1}{2}, d = 0 \tag{38}$$

second derivative

$$\alpha = 11, a = 13, b = -27, c = 15, d = -1, e = 0. \tag{39}$$

As the scheme has a very low numerical dissipation, the high wavenumber instabilities are not damped. This is especially true in reactive multicomponent mixture. Hence, in the simulation of the reacting mixing layer, filtering techniques are used (Lele, 1992). The general filtering scheme along i direction is

$$\alpha \tilde{f}_{i-1} + \tilde{f}_i + \alpha \tilde{f}_{i+1} = a f_i + \frac{d}{2}\left(f_{i+3} + f_{i-3}\right) + \frac{c}{2}\left(f_{i+2} + f_{i-2}\right) + \frac{b}{2}\left(f_{i+1} + f_{i-1}\right), \tag{40}$$

where $\tilde{f}_i$ is the filtered value. By imposing the scheme to be sixth order accurate, the Taylor series expansion gives the following relations for the coefficients

$$\begin{aligned} a &= \frac{1}{16}\left(11 + 10\alpha\right), \; b = \frac{1}{32}\left(15 + 34\alpha\right), \\ c &= \frac{1}{16}\left(-3 + 6\alpha\right), \; d = \frac{1}{32}\left(1 - 2\alpha\right). \end{aligned} \tag{41}$$

Hence, a one-parameter schemes family is obtained where α value determines the amount of waves to be filtered. In this work, α is imposed equal to 0.435, as this value ensures that the undesired instabilities are damped.

3.2 The temporal discretization

Equation 1 is advanced in time by using an explicit compact storage fourth order Runge-Kutta (RK) scheme (Gill, 1951) regarding the convective and diffusive terms, while the source term is solved in an implicit fashion. Hence, by writing Eq. 1 in the following compact form

$$\frac{\partial \mathbf{W}}{\partial t} = f\left(\mathbf{W}\right), \tag{42}$$

the RK scheme computes the $\mathbf{W}$ value at the new time step, $\mathbf{W}^{n+1}$, from the value at the old time step, $\mathbf{W}^{n}$, through 4 stages. In each stage, the computation of f is performed by using an implicit method for the source term, as described by Viggiano (2009).

4. The computational setup

The simulations of the reacting mixing layer are performed by using a rectangular computational domain. The streamwise dimension of the domain is equal to 1.5 cm, while the transverse one is chosen in order to avoid that the perturbation due to mixing reach the boundaries. Hence, by assuming a presumed value of the spreading rate of the mixing layer, based upon experimental studies in the literature, a ratio between the streamwise and transverse dimensions is fixed and the latter is computed from the former. Therefore, the transverse dimension is 0.4 cm in this computational case.

The domain is discretized by using a uniform mesh with cells of 40 μm. The aspect ratio of the cells is equal to 1, as the high gradients in all directions due to combustion require spatial accuracy in the stream direction as well as in the transverse one.

The order of magnitude of the computational time step, Δt, is $\mathcal{O}(10^{-5}$ ms$)$ to satisfy numerical stability for explicit schemes. If the highest temperature in the domain exceeds 1300 K, the Δt is reduced to $\mathcal{O}(10^{-6}$ ms$)$ in order to deal with the strong stiffness of the equations at high temperatures.

As the boundary conditions are concerned, the Navier-Stokes Characteristic Boundary Conditions (NSCBC) (Poinsot & Lele, 1992), extended to multicomponent flows (Abraham & Magi, 1997), are used. It was shown that these conditions give good results in the simulation of high Reynolds number flows as well as of high viscous flows (Poinsot & Lele, 1992). In the simulations presented in the following section, a subsonic inflow condition is imposed on the inlet boundary, while partially non-reflecting conditions are used on the remaining boundaries. The inlet mean velocities of n-heptane and air streams are imposed equal to 10 m/s and 3.82 m/s, respectively.

As the initial conditions are concerned, the mixing layer between two streams of air and fuel with different mean streamwise velocity is considered. The two layers velocities merge by means of a hyperbolic tangent profile. Near the splitter plate, a disturbance (Michalke, 1964) is superimposed on the flow field. The amplitude of the disturbance, v', is expressed by means of an exponential function, thus limiting the instability to the neighbourhood of the splitter plate

$$v' = 1.2\mathrm{e}^{-\frac{\left(x-\frac{L}{2}\right)^2}{2\left(\frac{\vartheta_i}{3}\right)^2}}\left[\sin\left(2\pi\frac{t}{P}\right)+\sin\left(\pi\frac{t}{P}\right)+\sin\left(\frac{2}{3}\pi\frac{t}{P}\right)\right], \tag{43}$$

where x is the transverse coordinate, L is the transverse dimension of the domain, ϑ_i is the initial momentum thickness, assumed equal to 0.0003 m, and P is the period of the fundamental harmonic, equal to $2 \cdot 10^{-1}$ ms. The hyperbolic tangent profile is also used to set the initial

density field. The initial value of pressure is equal to 40.5 bar and the initial temperature is 1000 K in the entire domain.
n-Heptane is chosen as model fuel and the 4-step mechanism, described by Muller *et al*. (1992), is used to model the autoignition. This mechanism was derived starting from a 1011 elementary reactions mechanism involving 171 chemical species. By using steady state assumptions for some intermediate species, a mechanism of 16 global reactions is obtained, that is controlled by the original elementary kinetic rates. Finally, the 16 reactions were reduced to the following 4 global steps

$$\begin{aligned} \mathrm{F} &\overset{1}{\Longrightarrow} \mathrm{X} \\ \mathrm{X} + 11\mathrm{O_2} &\overset{2}{\Longrightarrow} \mathrm{P} \\ \mathrm{F} + 2\mathrm{O_2} &\overset{3}{\Longleftrightarrow} \mathrm{I} \\ \mathrm{I} + 9\mathrm{O_2} &\overset{4}{\Longrightarrow} \mathrm{P} \end{aligned} \tag{44}$$

where F is the fuel, X stands for $3C_2H_4 + CH_3 + H$, I for $HO_2C_7H_{13}O + H_2O$ and P is the product resulting from the reactions, i.e. $7CO_2 + 8H_2O$. The reactions above are not the elementary ones, so an adjusted kinetic model is needed.
The 4-step mechanism is an attempt to describe, with a very small number of reactions, the chain branching at low temperature as well as the decomposition and subsequent oxidation of hydrocarbons at high temperature. The global reaction 3 is representative of the chain propagation process. The reaction 4 describes the chain branching and the subsequent oxidation to the final products. The activation energy of the reverse reaction $3b$ is higher than the forward one, $3f$. This ensures that at low temperature the reaction $3f$ is faster than $3b$. At high temperature, the backward reaction becomes dominant, thus leading to the transition from the first stage of ignition to the second one. The reaction 1 becomes important and leads to the decomposition of the fuel into the C_2H_4 and CH_3 hydrocarbons and H radicals. Finally, the reaction 2 describes the oxidation to the reaction products.
The simulations of the mixing layer are performed by using the following procedure. A non-reacting mixing layer between two streams of air and fuel is initially developed up to 1.8 ms from the start of computation. This time is sufficient in order to obtain a fully-developed mixing layer. Then, the time is reset to zero and chemical reactions are numerically switched on. In such a way, t_{ig} gives the chemical delay, that is comparable with the delay time obtained in a zero-dimensional configuration, if the initial composition and temperature of the mixed reactants are the same as in the two-dimensional case.
The ignition delay time is defined as the time when the following condition is satisfied (Viggiano & Magi, 2004)

$$\frac{dT}{dt} = 6 \cdot 10^6 \frac{K}{s}. \tag{45}$$

In two-dimensional simulations, Eq. 45 is used with T equal to the maximum value of temperature in the domain, $T_{\max}$.

5. Results

Figure 1 shows the temperature and density field of the developed mixing layer at $t = 1.8$ ms. As a consequence of the initial perturbation at the splitter plate, vortices are formed. While the mixing layer grows in the streamwise direction, the stream of fuel sweeps away the surrounding air and the contours at constant density are wrinkled. The overall effect is the air

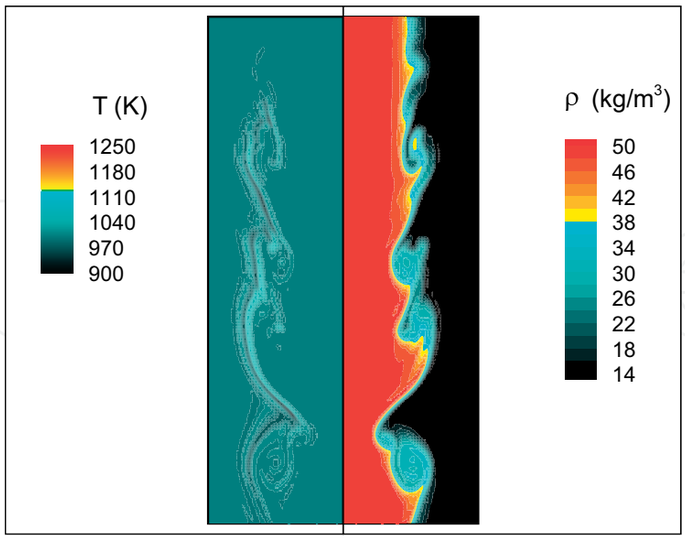

Fig. 1. Temperature and density field in a developed mixing layer.

entrainment in the fuel stream. As a consequence of the high strain rate in the mixing region, temperature locally increases, reaching the maximum value of 1070 K in the domain.
The ignition phenomenon is analysed by starting from the flow configuration shown in Fig. 1. Figure 2 shows the results in terms of contour lines at constant temperature (on the left) and fuel mass fraction (on the right) at three times. The time is computed from the numerical activation of the chemical reactions. In the frames, the white line corresponds to the isoline of stoichiometric mixture fraction ($Z = 0.062$). The figure shows that the temperature increases in some zones on the rich side of the mixture, close to the stoichiometric conditions. In these ignition spots, temperature increases slowly, at first, and then more rapidly.
As the localization of ignition spots is concerned, Fig. 2 shows that the most reactive zones correspond to regions where the temperature was higher at the start of the computation when chemistry was switched on. In this case, temperature is a key factor for the ignition to occur. This is in agreement with the results in the literature (Muller *et al.*, 1992; Viggiano & Magi, 2004) concerning the dependence of the ignition delay time on temperature in zero-dimensional configuration. The 4-step mechanism does not capture the NTC and t_{ig} is always reduced by increasing the temperature.
Besides, by analysing the contour lines at constant fuel mass fraction in the same figure, the ignition spots are found where a suitable rate between air and fuel occurs. This second condition is satisfied in the wrinkled interface between the two streams and in some small regions in the fuel stream, where air entrainment is more effective.
In Fig. 3 the values of mixture fraction characterizing the high temperature reactive zones are picked out by plotting the temperature versus mixture fraction in each computational grid point for several times. In this work, the mixture fraction, Z, is computed as the ratio between the mass of hydrogen and carbon and the total mass of the mixture. The increase of temperature is spread over a wide range of mixture fraction values, $0.18 < Z < 0.24$, up to $t = 0.08$ ms. Then, the combustion is shifted towards richer mixture.
The ignition delay time is equal to 0.11 ms.

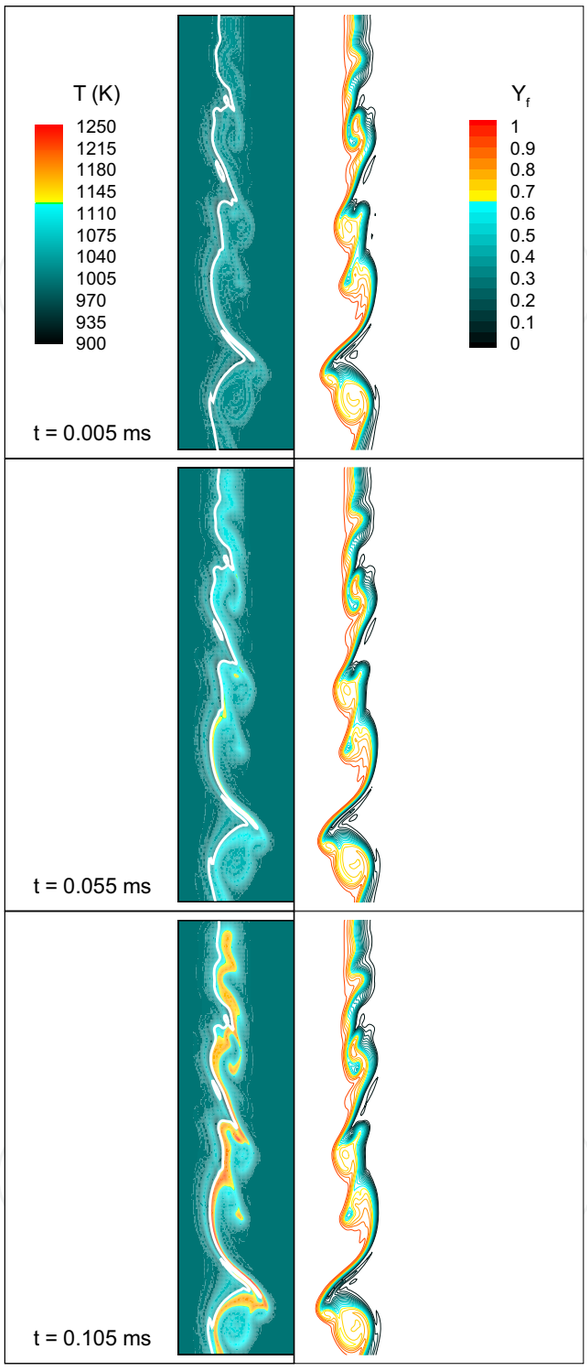

Fig. 2. Autoignition in a developed mixing layer: contours at constant temperature and fuel mass fraction at different times. The stoichiometric conditions are shown with a white line.

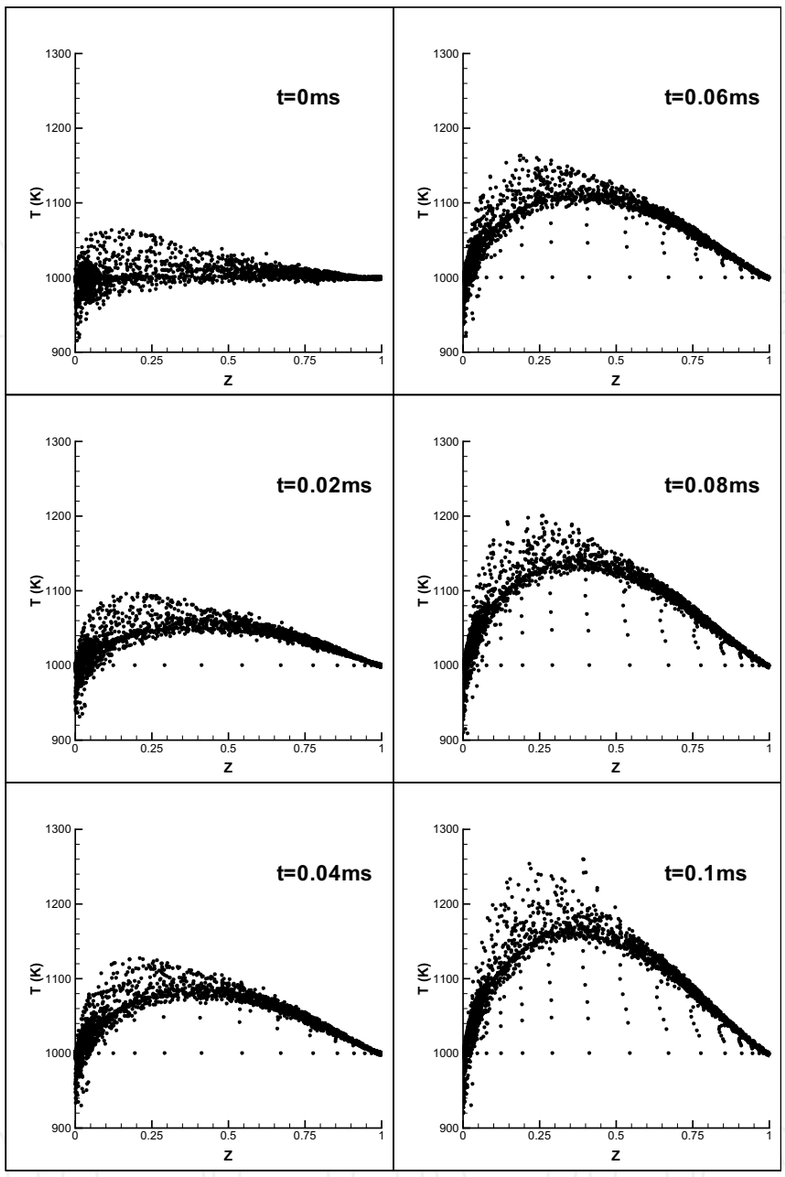

Fig. 3. Autoignition in a developed mixing layer: scatter plots of temperature versus mixture fraction.

Therefore, zero-dimensional simulations are performed in order to make a comparison with the results of the two-dimensional code. The initial conditions of the zero-dimensional computations are set equal to the most reactive conditions in the two-dimensional developed mixing layer, thus $T = 1070$ K and $0.18 < Z < 0.24$. The t_{ig} varies from 0.1 ms for $Z = 0.18$ to 0.07 ms for $Z = 0.24$. These results are in good agreement with the two-dimensional ones. The small differences are likely due to a non uniform value of Z in the ignition regions for the two-dimensional case.

6. Conclusions and further reading

A DNS methodology, coupled with accurate numerical schemes and proper combustion models, for the analysis of non-premixed reacting flows is presented. This numerical approach allows a comprehensive simulation of the physical process, as, by using proper computational grids, it accurately captures both the fluid dynamics and the chemistry scales of the phenomena.

In this work, the proposed methodology is used for the simulation of the ignition in a mixing layer, developed between two streams of air and *n*-heptane in a high pressure environment, thus assessing the potentiality of the software package. The results, in terms of ignition delay time and most reactive mixture fraction, are consistent with the thermochemistry of the problem, as confirmed by zero-dimensional computations. Besides, the role of temperature and of mixture fraction in determining the evolution of ignition is shown.

The same methodology was used by Viggiano & Magi (2004) for the study of ignition in a transient jet. The localization of the ignition spots was investigated and the effect of some physical parameters, such as the initial temperature of fuel and air and the velocity of the jet, was shown. The reader is referred to that work for further details.

Besides, the role of chemical kinetic mechanisms and of fluid dynamics on the ignition in transient jets was further explored by Viggiano (2009), by implementing more detailed mechanisms for the oxidation of *n*-heptane in the same software package. The employment of a detailed kinetic mechanism is fundamental if the initial temperature of the reactants is equal or higher than about 800 K. For lower temperature values, the fluid dynamics is determining in the localization of ignition spots and even a global mechanism, such as the 4-step one, could give reliable results.

7. References

Abraham, J. & Magi, V. (1997). Exploring Velocity Ratio and Density Ratio Effects in a Mixing Layer Using DNS. *International Journal of Computational Fluid Dynamics*, 8, 147-151.

Bilger, R.W.; Pope, S.B.; Bray, K.N.C. & Driscoll, J.F. (2005). Paradigms in turbulent combustion. *Proceedings of the Combustion Institute*, 30, 21-42.

Coffee, T.P. & Heimerl, J.M. (1981). Transport Algorithms for Premixed Laminar, Steady-State Flames. *Combustion and Flame*, 43, 273-289.

Gill, S. (1951). A Process for the Step-by-Step Integration of Differential Equations in an Automatic Computing Machine. *Proc. Cambridge Phil. Soc.*, 47, 96-108.

Glassman, I. (1996). *Combustion*, Academic Press, 3rd edition, ISBN: 978-0122858529.

Gordon, S. & McBride, B.J. (1971). Computer Program for Calculation of Complex Chemical Equilibrium Compositions, Rocket Performance, Incident and Reflected Shocks and Chapman-Jouguet Detonations. NASA report SP-273.

Hilbert, R.; Tap, F.; El-Rabii, H. & Thévenin, D. (2004). Impact of detailed chemistry and transport models on turbulent combustion simulations. *Progress in Energy and Combustion Science*, 30, 61-117.

Hirschfelder, J.O.; Curtiss, C.F. & Byron Bird, R. (1964). *The Molecular Theory of Gases and Liquids*, John Wiley & Sons, ISBN: 978-0471400653.

Kuo, K. (2005). *Principles of Combustion*, Wiley-Interscience, 2nd edition, ISBN: 978-0471046899.

Lele, S.K. (1989). Direct Numerical Simulation of Compressible Free Shear Flows, *AIAA Paper 89-0374*.

Lele, S.K. (1992). Compact Finite Difference Schemes with Spectral Like Resolution. *Journal of Computational Physics*, 103, 16-42.

Magi, V. (2004). Private Communications.

Mastorakos, E.; Baritaud, T.A. & Poinsot, T.J. (1997). Numerical Simulations of Autoignition in Turbulent Mixing Flows. *Combustion and Flame*, 109, 198-223.

Mastorakos, E. (2009). Ignition of turbulent non-premixed flames. *Progress in Energy and Combustion Science*, 35, 57-97.

Michalke, A. (1964). On the Inviscid Instability of the Hyperbolic Tangent Velocity Profile *Journal of Fluid Mechanics*, 19, 543-556.

Moin, P. & Mahesh, K. (1998). Direct Numerical Simulation: A Tool in Turbulence Research. *Annual Review of Fluid Mechanics*, 30, 539-578.

Muller, U.C., Peters, N. & Liñán, A. (1992). Global Kinetics for N-Heptane Ignition at High Pressure. *Proceedings of the Combustion Institute*, 24, 777-784.

Pitsch, H. (2006). Large-Eddy Simulation of Turbulent Combustion. *Annual Review of Fluid Mechanics*, 38, 453-482.

Poinsot, T.J. & Lele, S.K. (1992). Boundary Conditions for Direct Simulations of Compressible Viscous Flows. *Journal of Computational Physics*, 101, 104-129.

Sreedhara, S. & Lakshmisha, K.N. (2000). Direct Numerical Simulation of Autoignition in a Non-Premixed, Turbulent Medium. *Proceedings of the Combustion Institute*, 28, 25-34.

Viggiano, A. & Magi, V. (2004). A 2-D Investigation of the *n*-Heptane Autoignition by means of Direct Numerical Simulation. *Combustion and Flame*, 137, 432-443.

Viggiano, A. (2009). Exploring the Effect of Fluid Dynamics and Kinetic Mechanisms on *n*-Heptane Autoignition in Transient Jets. *Combustion and Flame*, doi:10.1016/j.combustflame.2009.10.004.

IntechOpen

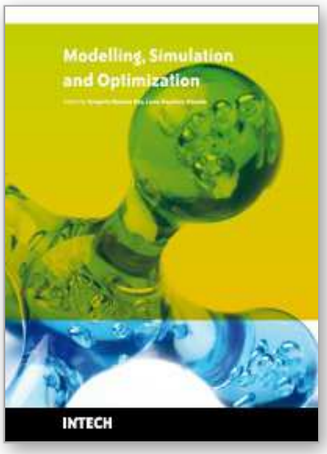

Modelling Simulation and Optimization

Edited by Gregorio Romero Rey and Luisa Martinez Muneta

ISBN 978-953-307-048-3
Hard cover, 708 pages
Publisher InTech
Published online 01, February, 2010
Published in print edition February, 2010

Computer-Aided Design and system analysis aim to find mathematical models that allow emulating the behaviour of components and facilities. The high competitiveness in industry, the little time available for product development and the high cost in terms of time and money of producing the initial prototypes means that the computer-aided design and analysis of products are taking on major importance. On the other hand, in most areas of engineering the components of a system are interconnected and belong to different domains of physics (mechanics, electrics, hydraulics, thermal...). When developing a complete multidisciplinary system, it needs to integrate a design procedure to ensure that it will be successfully achieved. Engineering systems require an analysis of their dynamic behaviour (evolution over time or path of their different variables). The purpose of modelling and simulating dynamic systems is to generate a set of algebraic and differential equations or a mathematical model. In order to perform rapid product optimisation iterations, the models must be formulated and evaluated in the most efficient way. Automated environments contribute to this. One of the pioneers of simulation technology in medicine defines simulation as a technique, not a technology, that replaces real experiences with guided experiences reproducing important aspects of the real world in a fully interactive fashion [iii]. In the following chapters the reader will be introduced to the world of simulation in topics of current interest such as medicine, military purposes and their use in industry for diverse applications that range from the use of networks to combining thermal, chemical or electrical aspects, among others. We hope that after reading the different sections of this book we will have succeeded in bringing across what the scientific community is doing in the field of simulation and that it will be to your interest and liking. Lastly, we would like to thank all the authors for their excellent contributions in the different areas of simulation.

InTech Europe
University Campus STeP Ri
Slavka Krautzeka 83/A

InTech China
Unit 405, Office Block, Hotel Equatorial Shanghai
No.65, Yan An Road (West), Shanghai, 200040, China

51000 Rijeka, Croatia
Phone: +385 (51) 770 447
Fax: +385 (51) 686 166
www.intechopen.com

中国上海市延安西路65号上海国际贵都大饭店办公楼405单元
Phone: +86-21-62489820
Fax: +86-21-62489821

IntechOpen

IntechOpen